*J. Fluid Mech.* (1993), *vol.* 246, *pp.* 489–502



# Frequency spectra of reactant fluctuations in turbulent flows

By GEORGE KOSÁLY

Department of Mechanical Engineering, University of Washington, Seattle, WA 98195, USA

(Received 8 October 1991 and in revised form 8 July 1992)

Bilger, Saetran & Krishnamoorthy (1991) give measured values of the variance, cross-correlation coefficient, autospectra, coherence and phase shift of the reactant concentration fluctuations for an irreversible second-order reaction in an incompressible turbulent scalar mixing layer. The present paper approaches the interpretation of the measured data by evaluating the above quantities in the frozen (slow) and equilibrium (fast) chemistry limits. We assume that the limiting values bracket the corresponding intermediate rate data.

The analysis leads to values that correspond with the measured variances and correlation coefficients. The paper offers simple procedures for experimenters to evaluate the fast chemistry limit of the spectral characteristics from the measured mixture fraction fluctuations. The investigation of the limiting spectra suggests that, in the frequency region considered in the Bilger *et al.* measurements, the shape of the autospectrum is quite insensitive to the chemistry rate. The cross-spectrum is much more sensitive to the chemistry than the autospectrum. The analysis predicts correctly that the coherence decreases with increasing frequency while the phase stays equal to $\pi$ until the decrease of the coherence leads to indeterminate phase results.

## 1. Introduction

The recent paper of Bilger, Saetran & Krishnamoorthy (1991, hereinafter referred to as BSK) investigates a reacting scalar mixing layer. Figure 1 shows a schematic of the experiment. Figure 2 shows the measured Eulerian time spectra (frequency spectra) of the reactant concentration fluctuations, and figure 3 shows the measured coherence and the phase between the reactant fluctuations. Figures 1, 2, and 3 are taken from BSK. The data published in BSK refer to two different chemistry rates characterized by the Damköhler number based on the large scale ($Da = 0.3$, 1.8). Figures 2 and 3 refer to the $Da = 0.3$ case. For further details see BSK.

The influence of first- and second-order isothermal reactions on the scalar spectra has been discussed by Corrsin (1961, 1964). Further discussion of the second-order case can be found in the review of Bilger (1980). The experimental spectral results of BSK shown in figures 2 and 3 refer to the middle of the flow ($y = 0$). The chemistry is $A + B \rightarrow$ products with negligible heat release. The initial mole fractions of the reactants ($\Gamma_{A_1}$, $\Gamma_{B_2}$) differ by only 3%, and the stoichiometric value of the mixture fraction ($F_s$) is close to 0.5.

Since the present work is to be compared with the data of BSK, it is therefore assumed here that $\Gamma_{A_1} = \Gamma_{B_2} = \Gamma_\infty$, $F_s = 0.5$, and that the flow is incompressible. The theoretical results are applicable at the middle of a reacting mixing layer and to

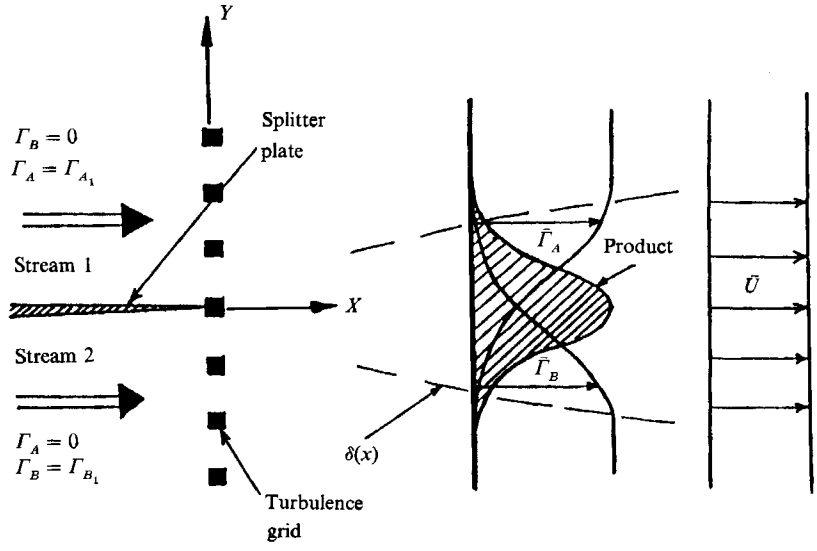


FIGURE 1. Schematic diagram of the reacting mixing layer. (This figure is taken from BSK.)

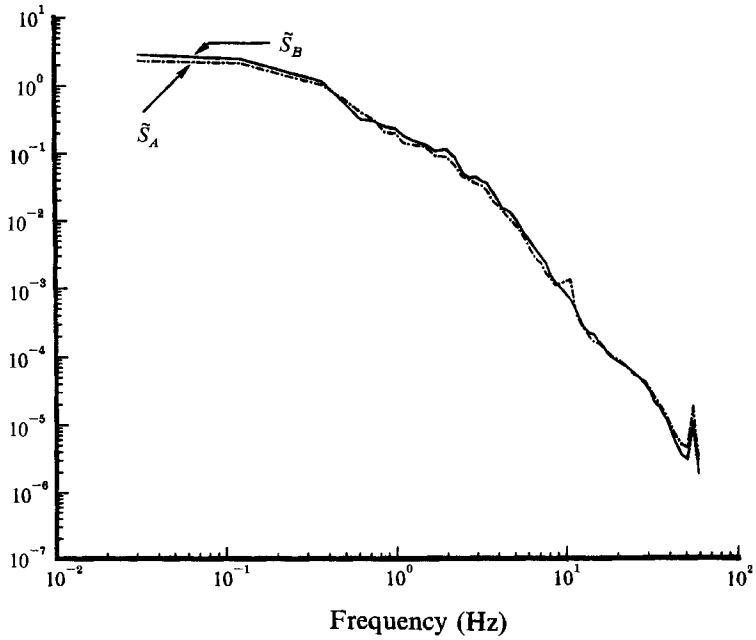


FIGURE 2. Measured autospectra of the reacting species at the middle of a scalar mixing layer; $x/M = 21$, $Da = 0.3$ (this figure is taken from BSK).

mixing and reaction in homogeneous flow behind a grid (Bennani, Gence & Mathieu 1985).

No theory exists at present that would satisfactorily predict the auto- and cross-spectra of the species concentration fluctuations for second-order reactions in turbulence (Corrsin 1961, 1969; Bilger 1980). In BSK the finite chemistry data are explained by bracketing them with the respective frozen and fast (equilibrium) chemistry limits. However, since the equilibrium limit of the reactant spectra is not

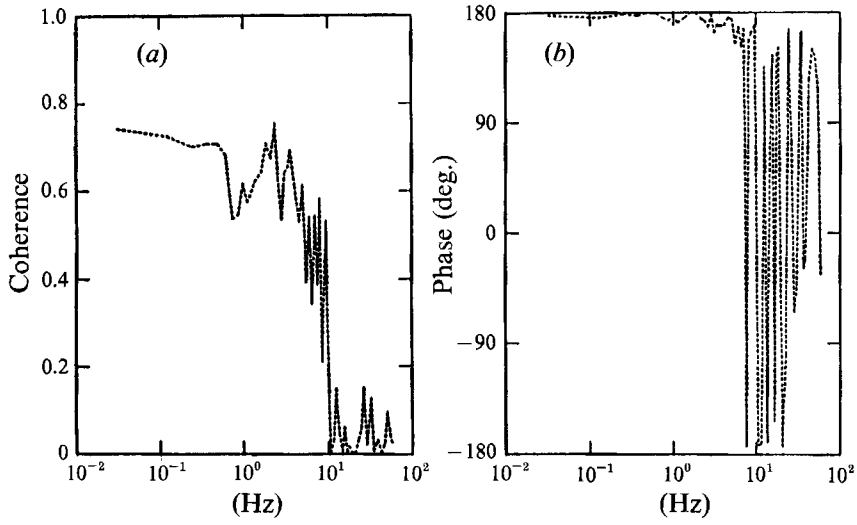


FIGURE 3. Measured coherence and phase at the middle of a scalar mixing layer; $x/M = 21$, $Da = 0.3$ (this figure is taken from BSK).

available in the literature, the spectral data shown in figures 2 and 3 remained unexplained in BSK.

The main goal of this work is to derive results that help understand the behaviour seen in figures 2 and 3, and to suggest new measurements to test some of the conclusions. We develop predictions in the frozen and in the equilibrium chemistry limits that correspond with the experimental results using the spectra of a conserved scalar (mixture fraction) and its absolute value. The analysis corresponds with the measured variances and correlation coefficients. The discussion suggests that, in the frequency region considered in the BSK measurements, the shape of the reactant autospectrum is quite insensitive to the Damköhler number. It is the cross-spectrum (coherence and phase) of the concentration fluctuation of the two reactants that is sensitive to the chemistry. While the coherence is predicted to decrease with frequency more rapidly with increasing reaction rate, the phase shift is expected to be equal to $\pi$ for arbitrary Damköhler number.

Section 2 refers to an arbitrary chemistry rate. Sections 3 and 4 discuss the limiting cases of frozen (slow) and equilibrium (fast) chemistry. It turns out that the limiting spectra are related in a rather simple way to the spectra of the mixture fraction fluctuations and the absolute value of the mixture fraction fluctuations. Section 5 discusses these two mixture fraction spectra. Section 6 applies measured mixture fraction data to evaluate the limiting reactant spectra which are, in turn, compared to the data in figures 2 and 3. Section 7 summarizes the conclusions and discusses possible further work.

## 2. Arbitrary chemistry rate

Using standard notation (see BSK) the mole fractions of the reactants ($\Gamma_i$) obey the equation

$$\mathscr{L}(\Gamma_i) \equiv \frac{\partial \Gamma_i}{\partial t} + \boldsymbol{U}\cdot\boldsymbol{\nabla}\Gamma_i - \boldsymbol{\nabla}\cdot(D\boldsymbol{\nabla}\Gamma_i) = -k\Gamma_A\Gamma_B, \quad i = A, B. \tag{1}$$

In the frozen (slow) chemistry limit we use the notation $\Gamma_i \equiv \Gamma_i^0$. Equation (1) becomes

$$\mathscr{L}(\Gamma_i^0) = 0, \quad i = A, B. \tag{2}$$

The reacting mixing layer is defined by the boundary conditions:

$$\Gamma_A(t, x = 0, y, z) = \Gamma_A^0(t, x = 0, y, z) = \begin{cases} \Gamma_\infty, & y > 0 \\ 0, & y < 0, \end{cases} \tag{3a}$$

$$\Gamma_B(t, x = 0, y, z) = \Gamma_B^0(t, x = 0, y, z) = \begin{cases} 0, & y > 0 \\ \Gamma_\infty, & y < 0, \end{cases} \tag{3b}$$

$$\Gamma_A(t, x, y, z)|_{y \to +\infty} = \Gamma_B(t, x, y, z)|_{y \to -\infty} = \Gamma_\infty,$$

$$\Gamma_A(t, x, y, z)|_{y \to -\infty} = \Gamma_B(t, x, y, z)|_{y \to +\infty} = 0.$$

The mixture fraction satisfies the equation

$$\mathscr{L}(F) = 0 \tag{4}$$

and the boundary conditions

$$F(t, x = 0, y, z) = \begin{cases} 1, & y > 0 \\ 0, & y < 0, \end{cases} \tag{5}$$

$$F(t, x, y, z)|_{y \to +\infty} = 1, \quad F(t, x, y, z)|_{y \to -\infty} = 0.$$

From (2), (3), (4) and (5)

$$\Gamma_A^0 = \Gamma_\infty F, \quad \Gamma_B^0 = \Gamma_\infty (1 - F). \tag{6}$$

Let us define

$$\Gamma_i^{\mathrm{ch}} \equiv \Gamma_i - \Gamma_i^0, \quad i = A, B. \tag{7}$$

$\Gamma_i^{\mathrm{ch}} (i = A, B)$ represents the influence of the chemistry on the concentrations. Using (1), (2), (3$a$, $b$), and (7) it follows that

$$\mathscr{L}(\Gamma_i^{\mathrm{ch}}) = -k \Gamma_A \Gamma_B, \tag{8}$$

$$\Gamma_i^{\mathrm{ch}}(t, x = 0, y, z) = 0, \quad i = A, B, \tag{9}$$

whence

$$\Gamma_A^{\mathrm{ch}} = \Gamma_B^{\mathrm{ch}} \equiv \Gamma_{\mathrm{ch}}. \tag{10}$$

Combining (6), (7), and (10) results in

$$\Gamma_A = \Gamma_\infty F + \Gamma_{\mathrm{ch}}, \quad \Gamma_B = \Gamma_\infty (1 - F) + \Gamma_{\mathrm{ch}}. \tag{11}$$

From now on we omit the ch subscript, and write $\Gamma_{\mathrm{ch}} \equiv \Gamma$.

Fluctuations are defined as

$$\Gamma_i = \bar{\Gamma}_i + \gamma_i, \quad i = A, B, \quad \Gamma = \bar{\Gamma} + \gamma, \quad F = \bar{F} + f. \tag{12}$$

The overbar denotes time average. Note again that $\Gamma \equiv \Gamma_{\mathrm{ch}}$, $\bar{\Gamma} \equiv \bar{\Gamma}_{\mathrm{ch}}$, $\gamma \equiv \gamma_{\mathrm{ch}}$. Definition (7) means that $\bar{\Gamma}$ is negative or zero.

From (11), (12)

$$\gamma_A = \Gamma_\infty f + \gamma, \quad \gamma_B = -\Gamma_\infty f + \gamma. \tag{13}$$

Equation (13) relates the fluctuations of the reactant concentrations to the fluctuation of the mixture fraction and a common fluctuating background due to chemistry.

The measured spectra are Eulerian time spectra. We define the auto- and cross-correlation functions of the reactant fluctuations as (Bendat & Piersol 1980)

$$\left.\begin{aligned} R_i(\tau, y) &= \overline{\gamma_i(t, x)\,\gamma_i(t+\tau, x)}, \\ R_{i,k}(\tau, y) &= \overline{\gamma_i(t, x)\,\gamma_k(t+\tau, x)}, \end{aligned}\right\} \quad i, k = A, B. \tag{14a}$$

$$\tag{14b}$$

(The notation suppresses the dependence on $x$.)

The auto- and cross-power spectral densities are defined via a Fourier transform as

$$S_i(\omega, y) = \int_{-\infty}^{+\infty} R_i(\tau, y)\, \mathrm{e}^{-\mathrm{i}\omega\tau}\, \mathrm{d}\tau, \quad S_{i,k}(\omega, y) = \int_{-\infty}^{+\infty} R_{i,k}(\tau, y)\, \mathrm{e}^{-\mathrm{i}\omega\tau}\, \mathrm{d}\tau. \tag{15a, b}$$

Since $R_{i,k}(\tau, y)$ is not necessarily an even function of $\tau$ the cross-spectrum is a complex quantity.

$$S_{i,k} = |S_{i,k}|\, \mathrm{e}^{-j\phi_{i,k}} \tag{15c}$$

defines the magnitude and the phase of the cross-spectrum (Bendat & Piersol 1980). The coherence between the concentration fluctuations of the reactants is defined as

$$C_{i,k} \equiv |S_{i,k}|^2/(S_i S_k). \tag{15d}$$

The coherence measures the relationship between the two signals as a function of frequency (Bendat & Piersol 1980).

Owing to the symmetry of the situation (cf. figure 1 and (3) and (5))

$$R_A(\tau, y) = R_B(\tau, -y) \quad \text{and} \quad R_{A,B}(\tau, y) = R_{B,A}(\tau, -y). \tag{16a, b}$$

Since $R_{B,A}(\tau, y) = R_{A,B}(-\tau, y)$ follows from the definition of the cross-correlation function (Papoulis 1984), (16$b$) can be rewritten as

$$R_{A,B}(\tau, y) = R_{A,B}(-\tau, -y). \tag{16c}$$

Equations (16$a, c$) show that at the centreline ($y = 0$)

$$R_A(\tau) = R_B(\tau), \quad R_{A,B}(\tau) = R_{A,B}(-\tau), \tag{17a, b}$$

whence

$$S_A(\omega) = S_B(\omega) \quad \text{and} \quad \phi_{A,B}(\omega) = 0 \quad \text{or} \quad \pi. \tag{18a, b}$$

The above results refer to $y = 0$ in the reacting mixing layer and are valid at any position in the homogeneous case. Equation (18$b$) follows from (15$b, c$) and (17$b$). Indeed if the cross-correlation function is even in $\tau$, the cross-spectrum becomes real. A real number can be positive or negative. $\phi_{A,B}(\omega) = 0$ or $\pi$ correspond to $S_{A,B}(\omega) > 0$ or $S_{A,B}(\omega) < 0$. Note that (18$a$, $b$) follow from the symmetry of the situation. For $y \neq 0$ the spectra of the two reactants are not equal and the phase can have values other than 0 or $\pi$. In the spatially homogeneous case (18$a, b$) are valid independently of the lateral position.

The prediction (18$b$) mirrors the experimental finding shown in figure 3, which demonstrates that $\phi_{A,B} = \pi$ for small frequencies where the coherence is high. This measured phase value is consistent with the prediction (18$b$) which, however, still allows that the phase be $\pi$ *or* zero. To explain why the measured phase is equal to $\pi$ we have to show that for low frequencies $S_{A,B} < 0$. We also have to demonstrate that the coherence decreases with frequency. The indeterminate nature of the experimental phase needs no separate discussion since low coherence necessarily results in indeterminate phase (Bendat & Piersol 1980). The sign of the cross-spectrum and the behaviour of the coherence will be discussed in §§4 and 6.

We conclude this section by expressing the auto- and cross-spectra by the spectra of the random processes $f$ and $\gamma$. Equation (13) shows that $\gamma_A$ and $\gamma_B$ depend linearly on $f$ and $\gamma$. Straightforward calculation leads to

$$S_A(\omega, y) = S_\gamma(\omega, y) + \Gamma_\infty^2 S_f(\omega, y) + \Gamma_\infty (S_{f,\gamma}(\omega, y) + \text{c.c.}), \tag{19a}$$

$$S_B(\omega, y) = S_\gamma(\omega, y) + \Gamma_\infty^2 S_f(\omega, y) - \Gamma_\infty (S_{f,\gamma}(\omega, y) + \text{c.c.}), \tag{19b}$$

$$S_{A,B}(\omega, y) = S_\gamma(\omega, y) - \Gamma_\infty^2 S_f(\omega, y) + \Gamma_\infty (S_{f,\gamma}(\omega, y) - \text{c.c.}). \tag{19c}$$

Here $S_{f,\gamma}(\omega, y)$ is the cross-spectrum of $f$ and $\gamma$. The notation suppresses the $x$-dependence. Complex conjugate is denoted by c.c.

Since at the middle of the flow (18$a$, $b$) are valid, the third terms on the right-hand sides vanish resulting in

$$S_A(\omega) = S_B(\omega) = S_\gamma(\omega) + \Gamma_\infty^2 S_f(\omega), \quad S_{A,B}(\omega) = S_\gamma(\omega) - \Gamma_\infty^2 S_f(\omega). \tag{20a, b}$$

Equations (20$a$, $b$) apply at the middle of a reacting mixing layer and to mixing and reaction in homogeneous flow behind a grid. $\phi_{A,B} = 0$ or $\pi$ correspond to $S_\gamma(\omega) > \Gamma_\infty^2 S_f(\omega)$ or $S_\gamma(\omega) < \Gamma_\infty^2 S_f(\omega)$.

To aid further discussion we write the cross-spectrum as

$$S_{A,B}(\omega) = S_A(\omega) - 2\Gamma_\infty^2 S_f(\omega),$$

whence

$$S_{A,B}(\omega)/S_A(\omega) = 1 - 2\Gamma_\infty^2 S_f(\omega)/S_A(\omega). \tag{21}$$

Let us denote by a tilde the auto-spectra normalized by the respective variances. Equations (20$a$) and (21) read

$$\tilde{S}_A(\omega) = \frac{\Gamma_\infty^2 \overline{f^2}}{\overline{\gamma_A^2}} \tilde{S}_f(\omega) + \frac{\overline{\gamma^2}}{\overline{\gamma_A^2}} \tilde{S}_\gamma(\omega), \quad \frac{S_{A,B}(\omega)}{S_A(\omega)} = 1 - \frac{2\Gamma_\infty^2 \overline{f^2}}{\overline{\gamma_A^2}} \frac{\tilde{S}_f(\omega)}{\tilde{S}_A(\omega)}. \tag{22a, b}$$

Note that $\bar{f} = \bar{\gamma} = 0$, therefore $\tilde{S}_f(\omega)$ and $\tilde{S}_\gamma(\omega)$ are the Fourier transforms of the respective autocorrelation coefficients of $f$ and $\gamma$. (For the definition of the autocorrelation coefficient of a variable, see Tennekes & Lumley 1972.)

Since the integral of the auto-spectrum for all frequencies is proportional to the variance, by integrating (20$a$) we obtain

$$\overline{\gamma_A^2} = \overline{\gamma^2} + \Gamma_\infty^2 \overline{f^2}. \tag{23}$$

Equations (22$a$, $b$) and (23) result in

$$\tilde{S}_A(\omega) = \frac{\Gamma_\infty^2 \overline{f^2}}{\Gamma_\infty^2 \overline{f^2} + \overline{\gamma^2}} \tilde{S}_f(\omega) + \frac{\overline{\gamma^2}}{\Gamma_\infty^2 \overline{f^2} + \overline{\gamma^2}} \tilde{S}_\gamma(\omega), \tag{24a}$$

$$\frac{S_{A,B}(\omega)}{S_A(\omega)} = 1 - 2 \Big/ \left[ 1 + \frac{\overline{\gamma^2}}{\Gamma_\infty^2 \overline{f^2}} \frac{\tilde{S}_\gamma(\omega)}{\tilde{S}_f(\omega)} \right]. \tag{24b}$$

Figure 2 shows the $\tilde{S}_A(\omega)$, $\tilde{S}_B(\omega)$ data. The coherence and the phase (for data see figure 3) are determined by the right-hand-side of (24$b$). The coherence is equal to the square of the absolute value of the right-hand-side. The sign of the right-hand-side determines whether the phase is zero or $\pi$.

A further quality of interest is the correlation coefficient between the reactant fluctuations:

$$R_{A,B}(y) = \overline{\gamma_A \gamma_B} / (\overline{\gamma_A^2 \gamma_B^2})^{\frac{1}{2}}. \tag{25a}$$

At the middle of the flow ($y = 0$)

$$R_{A,B} = \overline{\gamma_A \gamma_B}/\overline{\gamma_A^2}. \tag{25b}$$

## 3. The frozen chemistry limit

In this limit $\gamma = 0$ in (13), therefore

$$\overline{\gamma_A^2} = \Gamma_\infty^2 \overline{f^2}, \quad R_{A,B} = \frac{-\Gamma_\infty^2 \overline{f^2}}{\Gamma_\infty^2 \overline{f^2}} = -1, \tag{26a, b}$$

$$\tilde{S}_A(\omega) = \tilde{S}_f(\omega), \quad \frac{S_{A,B}(\omega)}{S_A(\omega)} = -1. \tag{26c, d}$$

Equations (26*c*, *d*) represent the frozen chemistry predictions relevant to figures 2 and 3. In this limit the auto-spectrum of the reactant fluctuations is equal to the auto-spectrum of the fluctuations of the mixture fraction. Equation (26*d*) predicts unit coherence and $\phi_{A,B}(\omega) = \pi$.

## 4. The equilibrium chemistry limit

If $F_s = 0.5$, then in the equilibrium chemistry limit (Bilger 1980)

$$\Gamma_A^e = 2\Gamma_\infty \begin{cases} F - 0.5 & \text{if } F > 0.5 \\ 0 & \text{if } F < 0.5, \end{cases} \qquad \Gamma_B^e = 2\Gamma_\infty \begin{cases} 0 & \text{if } F > 0.5 \\ 0.5 - F & \text{if } F < 0.5. \end{cases} \tag{27a}$$

Since at the middle of the flow $\bar{F} = 0.5$, $f = F - 0.5$, leading to

$$\bar{\Gamma}_A^e = \bar{\Gamma}_B^e = 2\Gamma_\infty \int_0^{0.5} \xi P_f(\xi)\, \mathrm{d}\xi = \Gamma_\infty \overline{|f|}. \tag{27b}$$

$P_f(\xi)$ is the probability density function (p.d.f.) of the random variable $f$ (Bilger 1980).

From (27*a*, *b*)

$$\left.\begin{aligned} \gamma_A^e = \Gamma_A^e - \bar{\Gamma}_A^e = \Gamma_\infty \begin{cases} 2f - \overline{|f|} & \text{if } f > 0 \\ -\overline{|f|} & \text{if } f < 0, \end{cases} \\ \gamma_B^e = \Gamma_B^e - \bar{\Gamma}_B^e = \Gamma_\infty \begin{cases} -\overline{|f|} & \text{if } f > 0 \\ -2f - \overline{|f|} & \text{if } f < 0, \end{cases} \end{aligned}\right\} \tag{28}$$

whence, upon insertion into (25*b*) it follows that

$$R_{AB}^e = -\overline{|f|}^2/(2\overline{f^2} - \overline{|f|}^2). \tag{29}$$

Sufficiently far from the inlet the p.d.f. of $f$ can be approximated by the normal distribution. (See for example, the measured kurtosis values in figure 7 of BSK.) In this approximation

$$\overline{|f|} = (2/\pi)^{\frac{1}{2}} (\overline{f^2})^{\frac{1}{2}}, \tag{30}$$

resulting in

$$R_{AB}^e = \frac{1}{1 - \pi} = -0.47. \tag{31}$$

This is the equilibrium chemistry prediction of the correlation coefficient. We turn now to the discussion of $\overline{\gamma^{2e}}$ and $\tilde{S}_\gamma^e(\omega)$. These quantities are needed to evaluate the auto- and cross-spectra from (24*a*, *b*).

From (11) and (27$a$) it follows that

$$\Gamma^{\mathrm{e}} \equiv \Gamma^{\mathrm{e}}_{\mathrm{ch}} = \Gamma_\infty \begin{cases} F-1 & \text{if} \quad F > 0.5 \\ -F & \text{if} \quad F < 0.5, \end{cases} \tag{32}$$

whence with (27$b$)

$$\bar{\Gamma}^{\mathrm{e}} \equiv \bar{\Gamma}^{\mathrm{e}}_{\mathrm{ch}} = \Gamma_\infty (\overline{|f|} - \tfrac{1}{2}). \tag{33}$$

$\gamma^{\mathrm{e}} \equiv \gamma^{\mathrm{e}}_{\mathrm{ch}} \equiv \Gamma^{\mathrm{e}} - \bar{\Gamma}^{\mathrm{e}}$ leads to

$$\gamma^{\mathrm{e}} = \Gamma_\infty (|f| - \overline{|f|}). \tag{34}$$

From (30) and (34)

$$\overline{\gamma^{2\mathrm{e}}} = \Gamma^2_\infty (\overline{|f|^2} - \overline{|f|}^2) = \Gamma^2_\infty (\overline{f^2} - \overline{|f|}^2) = \Gamma^2_\infty \overline{f^2}(1 - 2/\pi). \tag{35}$$

Since $\bar{\gamma} = 0$ we write the autocorrelation coefficient of $\gamma^{\mathrm{e}}$ as

$$\rho^{\mathrm{e}}_\gamma(\tau) = R^{\mathrm{e}}_\gamma(\tau) / \overline{\gamma^{2\mathrm{e}}}. \tag{36}$$

$R^{\mathrm{e}}_\gamma(\tau)$ is the autocorrelation function of the $\gamma^{\mathrm{e}}$ variable.

Using (34) in (36), straightforward calculation results in

$$\rho^{\mathrm{e}}_\gamma(\tau) = \frac{R_{|f|}(\tau) - \overline{|f|}^2}{\overline{f^2} - \overline{|f|}^2} \equiv \rho_{|f|}(\tau), \tag{37}$$

which is equivalent to

$$\tilde{S}^{\mathrm{e}}_\gamma(\omega) = \tilde{S}_{|f|}(\omega). \tag{38}$$

The random process $\gamma$ is the fluctuation of the 'chemistry background' defined in (7). (See also (13).) In the fast chemistry limit at the middle of a scalar mixing layer (and at an arbitrary lateral position for the spatially homogeneous case), the normalized autospectrum of the $\gamma$ process is identical to the normalized autospectrum of the absolute value of the mixture fraction fluctuation. (In the rest of the paper the terms '$f$-process' and '$|f|$-process' respectively will be used.) Insertion of (35) and (38) into (24$a, b$) results in

$$\tilde{S}^{\mathrm{e}}_A(\omega) = \frac{\pi}{2(\pi-1)} \tilde{S}_f(\omega) + \frac{\pi-2}{2(\pi-1)} \tilde{S}_{|f|}(\omega) = 0.73 \tilde{S}_f(\omega) + 0.27 \tilde{S}_{|f|}(\omega), \tag{39a}$$

$$\frac{S^{\mathrm{e}}_{AB}(\omega)}{S^{\mathrm{e}}_A(\omega)} = 1 - 2 \Big/ \left[ 1 + \frac{\pi-2}{\pi} \frac{\tilde{S}_{|f|}(\omega)}{\tilde{S}_f(\omega)} \right] = 1 - 2 \Big/ \left[ 1 + 0.36 \frac{\tilde{S}_{|f|}(\omega)}{\tilde{S}_f(\omega)} \right]. \tag{39b}$$

The results refer to the middle of a scalar mixing layer, sufficiently far from the inlet so that a Gaussian p.d.f. shall be applicable. Note that in the homogeneous case the results are valid independently of the lateral position.

To continue the derivation, $\tilde{S}_f(\omega)$ and $\tilde{S}_{|f|}(\omega)$ are needed. Once these spectra are known the autospectrum of the reactant fluctuations can be computed from (39$a$). The coherence and the phase between the reactant fluctuations are determined by the square of the absolute value and the sign of the right-hand side of (39$b$), respectively.

## 5. The spectra of $f$ and $|f|$

Equations (39$a, b$) show that in order to predict the behaviour of the reactant spectra in the equilibrium limit, one has to know $\tilde{S}_{|f|}(\omega)$ and $\tilde{S}_f(\omega)$. While it seems impossible to derive a closed-form expression linking $\tilde{S}_{|f|}(\omega)$ and $\tilde{S}_f(\omega)$, the respective autocorrelation coefficients can be expressed in terms of the other. Thomas (1969)

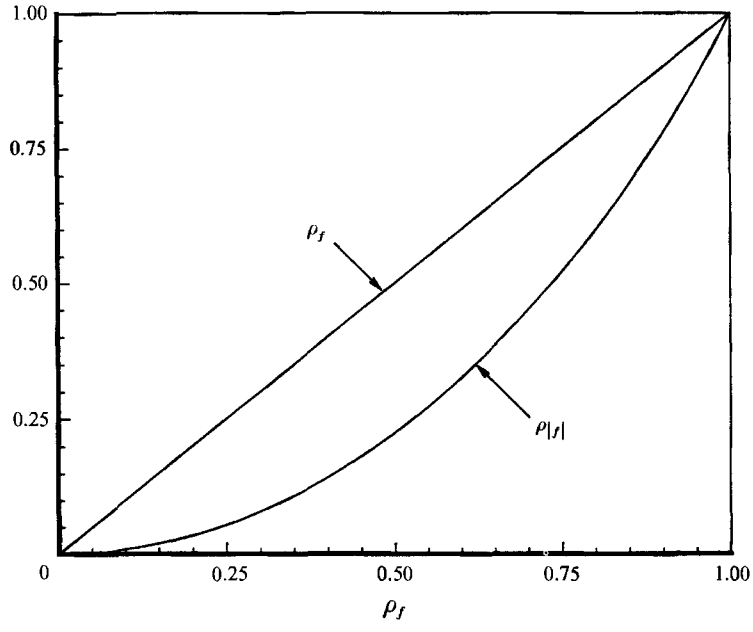


FIGURE 4. $\rho_{|f|}$ *vs.* $\rho_f$ as given by (41).

shows that if the $f$-process is stationary and normal, the autocorrelation function of $|f|$ can be written as

$$R_{|f|}(\tau) = \frac{2}{\pi}\overline{f^2}\,[\rho_f(\tau)\arcsin\rho_f(\tau) + (1-\rho_f^2(\tau))^{\frac{1}{2}}]. \tag{40}$$

Insertion of (30) and (40) into (37) results in

$$\rho_{|f|}(\tau) = \frac{2}{\pi - 2}\,[\rho_f(\tau)\arcsin\rho_f(\tau) + (1-\rho_f^2(\tau))^{\frac{1}{2}} - 1]. \tag{41}$$

$\rho_f(\tau)$ is the autocorrelation coefficient of the mixture fraction fluctuation. From any known $\tilde{S}_f(\omega)$ spectrum $\rho_f(\tau)$ can be determined which, in turn, provides $\rho_{|f|}(\tau)$ through (41). $\tilde{S}_{|f|}(\omega)$ is the Fourier transform of $\rho_{|f|}(\tau)$.

Figure 4 shows $\rho_{|f|}$ versus $\rho_f$ as calculated from (41). Let $\mathscr{T}_f$ and $\mathscr{T}_{|f|}$ be the integral timescales of the $f$ and the $|f|$ processes:

$$\mathscr{T}_f = \int_0^\infty \rho_f(\tau)\,\mathrm{d}\tau, \quad \mathscr{T}_{|f|} = \int_0^\infty \rho_{|f|}(\tau)\,\mathrm{d}\tau \tag{42}$$

(Tennekes & Lumley 1972). Figure 4 shows that $\rho_{|f|}(\tau)$ decreases with $\tau$ faster than $\rho_f(\tau)$, therefore

$$\mathscr{T}_{|f|} < \mathscr{T}_f, \tag{43a}$$

whence

$$\tilde{S}_{|f|}(\omega = 0) < \tilde{S}_f(\omega = 0). \tag{43b}$$

($\tilde{S}_f(\omega = 0) = 2\mathscr{T}$ for any stationary process.) Since the area under any autospectrum normalized by its variance is equal to $\pi$ (Papoulis 1984), it follows from (43$b$) that $\tilde{S}_{|f|}(\omega)$ decreases with frequency more slowly than $\tilde{S}_f(\omega)$, which means that the two autospectra have to cross at some frequency, with the spectrum of $|f|$ extending to higher frequencies.

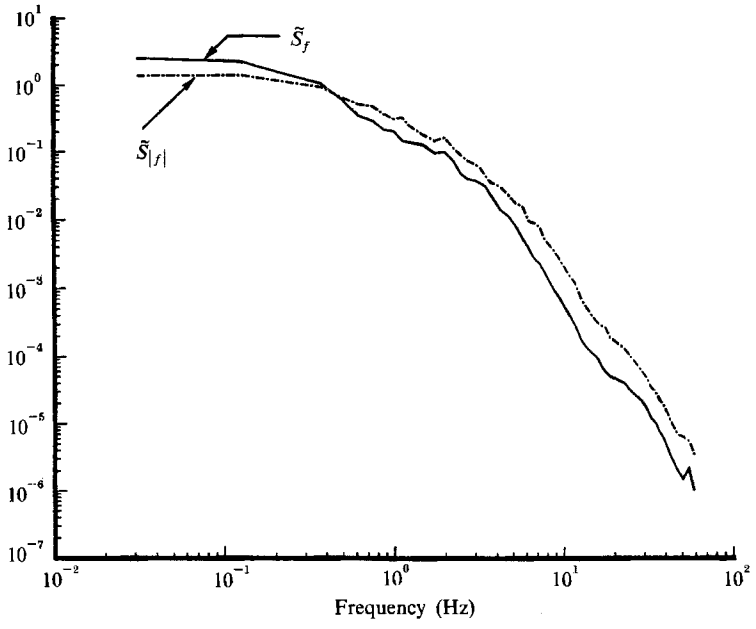


FIGURE 5. Measured spectra of $f$ and $|f|$; $x/M = 21$ (Bilger & Krishnamoorthy, 1991, personal communication).

Figure 5 shows measured spectra (R. W. Bilger & L. V. Krishnamoorthy 1991, personal communication)) of $f$ and $|f|$ referring to the same axial ($x/M = 21$) and radial position ($y = 0$) as figures 2 and 3. The behaviour of the curves in figure 5 mirrors the expectation deduced from (41). Note that it is quite natural that the $f$-signal contains higher frequencies than the $|f|$-signal since: (i) any smooth zero-crossing of $f$ creates a sharp dip in $|f|$; (ii) any periodicity of frequency $\omega$ in $f$ shows up at $2\omega$ in $|f|$.

## 6. Discussion and comparison to data

The data comparison given below is based on experimental results for the middle of a scalar mixing layer: $x/M = 21$, $Da = 0.3$. For more details see BSK. The theoretical results discussed in §§3–5 are also applicable to mixing and reaction in a spatially homogeneous case. Unfortunately no spectral data are available for reacting homogeneous flow.

The predictions given in §§3 and 4 refer to the frozen and the equilibrium chemistry limits. BSK discusses numerous cases when the two limiting cases bracket intermediate rate chemistry data. We will now use the results in §§3–5 to compare the variance, the correlation coefficient, the autospectra, and the coherence, of the concentration fluctuations of the reactants. Note that there is no mathematical proof that these quantities must be bracketed by their limiting values. We use this assumption as a physically plausible postulate (see BSK and Toor 1975). The phase shift of the cross-spectrum will be predicted to be equal to $\pi$ for arbitrary Damköhler number.

Equations (23), (26$a$), and (35) show that the variance of the mole fraction fluctuations is $2(1-1/\pi) = 1.36$ times higher in the fast chemistry limit than in the

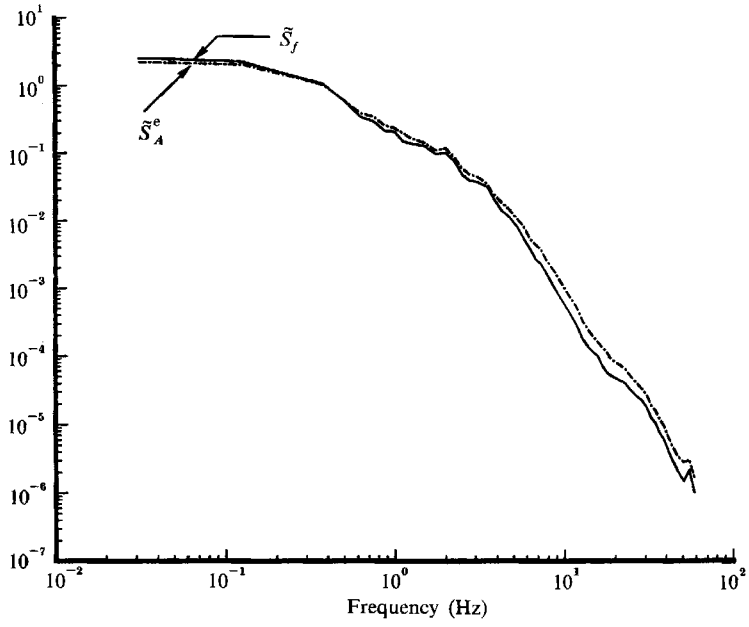


FIGURE 6. The frozen and the equilibrium limits of the reactant autospectrum. The curves have been computed from (26*c*) and (39*a*) using the figure 5 data.

frozen chemistry case, resulting in a 17% difference between the root mean squares. The prediction is confirmed by the data shown in figure 9 of BSK.

Equations (26*b*) and (31) indicate that for intermediate rate chemistry $-0.47 > R_{A,B} > -1$. (Here $-0.47$ is the fast chemistry limit, $-1$ is the frozen value.) $R_{A,B}$ is the correlation coefficient of the reactant fluctuations at the middle of the reaction layer. The experimental values of $R_{A,B}$ given in BSK are $-0.8$ and $-0.6$. These values refer to the middle of the flow at $x/M = 21$ and to the respective Damköhler number values of 0.30 and 1.81. The data clearly corroborate the prediction. Note that the above limiting values also bracket the finite rate chemistry results computed via the linear-eddy turbulent mixing model (Kerstein 1992).

Equation (39*a*) gives the auto-spectrum in the equilibrium limit as the 'weighted average' of the auto-spectra of $f$ and $|f|$. From (39*a*) and figure 5 it is obvious that $\tilde{S}_A^e(\omega = 0) < \tilde{S}_f(\omega = 0)$; therefore, the two spectra have to cross at some frequency. (Remember that the areas under both spectra are identical.) At high frequencies the reactant spectrum becomes larger than the mixture-fraction spectrum. This effect is due to the influence of the spatial width of the reaction region. Since this lengthscale is normally smaller than the large turbulence scales, it contributes to the spectrum at high wavenumber values, that is, at large frequencies.

Figure 6 shows the autospectrum of $f$ and the equilibrium limit of the reactant autospectrum as computed from (39*a*) using the figure 5 data. While the reactant spectrum indeed extends to higher frequencies the effect appears to be quite small. Since the two curves in figure 6 are expected to bracket the finite chemistry spectra, it is concluded that in the frequency range considered in the BSK measurements the shape of the autospectrum is not sensitive to the chemistry rate. The influence of the chemistry is probably much stronger at higher frequencies that cannot be seen in the data. Figure 2 exhibits the measured normalized autospectra of the two reactants at $Da = 0.3$ as given in BSK. Comparison of figures 2 and 6 demonstrates that at

around 10 Hz, where the frozen and equilibrium spectra start to differ, the figure 2 reactant spectra follow the equilibrium line. The $Da = 1.8$ autospectra are mentioned in BSK but are not yet available. The present prediction is that the $Da = 0.3$ and 1.8 autospectra will not differ significantly from each other.

The conclusion that the reactant autospectrum does not differ significantly from the mixture fraction spectrum follows from (39*a*) and figure 5. Equation (39*a*) is valid at the middle of a scalar mixing layer and at any lateral position in the spatially homogeneous case behind a grid, provided that the sensor is sufficiently far from the inlet so that the p.d.f. of $f$ is normal. The difference between $\tilde{S}_f$ and $\tilde{S}_A^e$ depends also on the deviation between $\tilde{S}_f$ and $\tilde{S}_{|f|}$ (figure 5). The frequencies where this deviation becomes large are probably well above the frequency region considered in the BSK measurements.

The present discussion refers to the frequency spectrum which can, however, be converted to the one-dimensional wavenumber spectrum for a mixing layer and can also be applied to determine the three-dimensional wavenumber spectrum for the spatially homogeneous case (Tennekes & Lumley 1972). In order to investigate further the sensitivity of the reactant autospectra to the Damköhler number, new data are needed both for the highly symmetrical cases discussed in §§3 and 4 and for more general conditions. The laboratory study of spatially homogeneous cases appears to be especially important. The generalization of (39*a*) to more complex situations is straightforward.

We turn now to the discussion of the coherence and the phase. Since $\tilde{S}_{|f|}(\omega = 0) < \tilde{S}_f(\omega = 0)$ (cf. §5) the left-hand side of (39*b*) is smaller at zero frequency than $1 - 2/1.36 = -0.47$, which means that it is negative; therefore the equilibrium prediction of the phase at $\omega = 0$ is $\pi$. Since $\tilde{S}_{|f|}(\omega)$ decreases with frequency more slowly than $\tilde{S}_f(\omega)$, with increasing frequency the second term on the right-hand side of (39*b*) decreases, therefore the right-hand side of (39*b*) increases. Since $S^e_{A,B}(\omega)/S^e_A(\omega)$ is negative at zero frequency, its increase with frequency leads to the decrease of its absolute value. It follows that in the equilibrium limit the coherence between the reactant fluctuations decreases with increasing frequency.

Theoretically the phase of the cross-spectrum remains $\pi$ as long as $S^e_{A,B}(\omega)/S^e_A(\omega) < 0$. (See the discussion after (18*b*) and (20*b*).) In practice, however, the drop in the coherence will result in indeterminate phase (Bendat & Piersol 1980). Equation (39*b*) shows that after the coherence drops to zero, further decrease of the ratio on the right-hand side of (39*b*) may result in increasing coherence, and $\phi^e_{A,B}(\omega) = 0$. Since this effect does not show in the data, for the time being, we do not discuss this possibility further.

The frozen line in figure 7 corresponds to (26*d*). The equilibrium limit of the coherence was computed from (39*b*) using the figure 5 data. Figure 7 demonstrates that the coherence between the two different reacting species depends quite sensitively on the reaction rate. The experimental values were taken from BSK and refer to the $Da = 0.3$ case. The data are bracketed by the two limits, as expected. The present prediction is that any $Da > 0.3$ data taken under the BSK conditions will fall between the equilibrium and the experimental curves shown in figure 7. The coherence curve corresponding to $Da = 1.8$ has been mentioned in BSK but is not yet available. When available it will provide a sensitive test of the present approach.

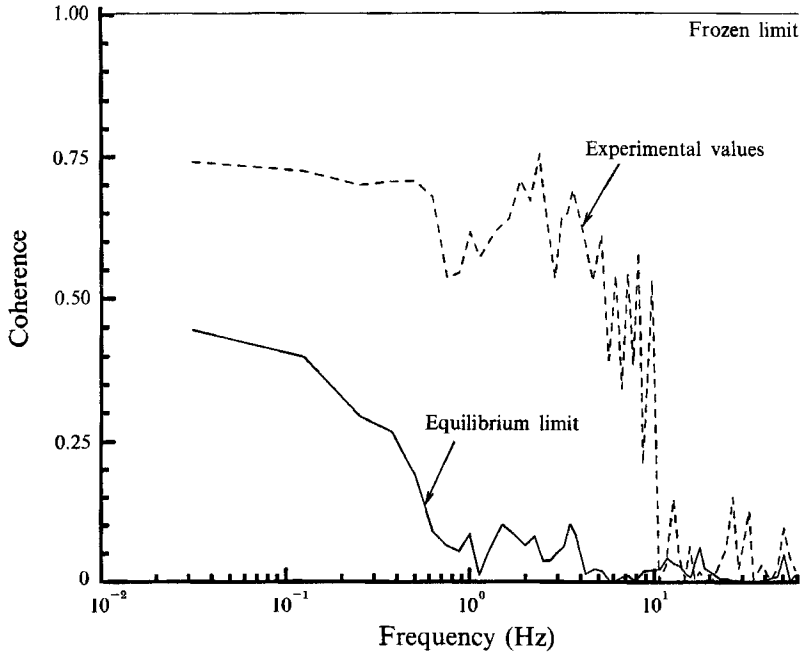


FIGURE 7. Coherence *vs.* frequency. The frozen and equilibrium limits have been computed from (26*d*) and (39*b*) using the figure 5 data. The experimental curve is taken from BSK and is identical to the curve shown in figure 3(*a*). $x/M = 21$, $Da = 0.3$).

## 7. Conclusions and further work

It is a common approach in the interpretation of turbulent reacting flow experiments to evaluate the frozen and equilibrium limits of the respective quantities and apply the limits to explain the finite chemistry results. BSK and the classical paper of Toor (1975) demonstrate that discussion via the limits is a fruitful way to gain insight into the main trends in the data.

The present work corroborates the variance and the correlation coefficient of the reactant fluctuations. More important than that are the results referring to the spectral characteristics. While in BSK the authors explain the rest of their finite chemistry data via limiting results, they could not follow this avenue regarding their spectral data since the equilibrium chemistry limit of the auto- and cross-spectra of the reactant concentration fluctuations was not available for application.

The main analytic results of the present work are (39*a*, *b*) which provide simple relationships to evaluate the equilibrium spectra from the spectra of $f$ (mixture fraction fluctuation) and $|f|$. While no theory exists at present that would satisfactorily predict reactant spectra, the evaluation of the spectrum of a passive scalar is a more standard task (Tennekes & Lumley 1972; Lesieur, Montmory & Chollet 1987). The spectrum of $f$ and $|f|$ are related to each other through (41).

R. W. Bilger & L. V. Krishnamoorthy (1991, personal communication) provided measured spectra of $f$ and $|f|$ so that (39*a*, *b*) could be applied for the interpretation of their results shown in figures 2 and 3. Using their data in conjunction with (26*c*) and (39*a*) shows that the two limiting normalized reactant autospectra nearly coincide. The finding suggests that, in the frequency region considered in the BSK measurements, the shape at the reactant autospectrum is not sensitive to the Damköhler number. The influence of the chemistry on the shape of the reactant

autospectrum is probably much stronger at higher frequencies that cannot be seen in the BSK data. This finding needs to be tested against further data. The coherence is found to decrease with increasing frequency and the phase is proved to be equal to $\pi$ until it becomes indeterminate due to small coherence. These conclusions are mathematical consequences of (39*b*). Using the data of Bilger & Krishnamoorthy (1991, personal communication) in (39*b*) resulted in the equilibrium curve shown in figure 7. Since the figure 7 experimental data refer to $Da = 0.3$, the prediction is that any $Da > 0.3$ result should fall between the $Da = 0.3$ data and the equilibrium prediction. Figure 7 demonstrates that in the frequency region considered, the cross-spectrum is more sensitive to the chemistry than the autospectrum.

The theoretical considerations in this paper refer to the middle of a reacting mixing layer and to arbitrary lateral position in the spatially homogeneous case. It is desirable that new measurements should be taken both in these highly symmetrical cases and under more general conditions.

The author is indebted to R. W. Bilger and L. V. Krishnamoorthy for making unpublished data available. Special acknowledgement is made of the helpful comments on the manuscript by R. W. Bilger. Thanks are due to J. A. Ritcey for drawing the author's attention to the valuable book of Thomas (1969). The work was jointly supported by NSF and AFOSR under NSF Contract No. CTS-9021928.

## REFERENCES

Bendat, J. S. & Piersol, A. G. 1980 *Engineering Applications of Correlation and Spectral Analysis*. John Wiley.

Bennani, A., Gence, J. N. & Matthieu, J. 1985 The influence of grid-generated turbulence on the development of chemical reactions. *AIChE J.* **31**, 1157.

Bilger, R. W. 1980 Turbulent flows with nonpremixed reactants. In *Turbulent Reacting Flows* (ed. P. A. Libby & F. A. Williams), pp. 65–113. Springer.

Bilger, R. W., Saetran, L. R. & Krishnamoorthy, L. V. 1991 Reaction in a scalar mixing layer. *J. Fluid Mech.* **233**, 211 (referred to herein as BSK).

Corrsin, S. 1961 The reactant concentration spectrum in turbulent mixing with a first order reaction. *J. Fluid Mech.* **11**, 407.

Corrsin, S. 1964 Further consideration of Onsager's cascade model for tubulent spectra. *Phys. Fluids* **7**, 1156.

Kerstein, R. A. 1992 Linear eddy modeling of turbulent transport. Part 7. Finite rate chemistry and multi-stream mixing. *J. Fluid Mech.* **240**, 289.

Lesieur, M., Montmory, C. & Chollet, J. P. 1987 The decay of kinetic energy and temperature variance in three-dimensional isotropic turbulence. *Phys. Fluids* **30**, 1278.

Papoulis, A. 1984 *Probability, Random Variables and Stochastic Processes* (2nd edn). McGraw-Hill.

Tennekes, H. & Lumley, J. L. 1972 *A First Course in Turbulence*. MIT Press.

Thomas, J. B. 1969 *An Introduction to Statistical Communication Theory*. John Wiley.

Toor, H. L. 1975 The non-premixed reaction: A + B → Products. In *Turbulence in Mixing Operations* (ed. R. S. Broadkey). Academic.